Water Air Soil Pollut (2017) 228: 278
DOI 10.1007/s11270-017-3461-y

Synthesis of a Quaternized Beta Cyclodextrin-Montmorillonite Composite and Its Adsorption Capacity for Cr(VI), Methyl Orange, and p-Nitrophenol

Anrong Zeng · **Anran Zeng**

Received: 24 March 2017 / Accepted: 27 June 2017 / Published online: 13 July 2017
© Springer International Publishing AG 2017

Abstract In this paper, quaternized β-cyclodextrin–montmorillonite composite (QCD-MMT) was obtained and absorption properties of Cr(VI), methyl orange and p-nitrophenol were studied. QCD was prepared by 2,3-epoxypropyltrimethylammonium chloride and β-cyclodextrin (β-CD). QCD-MMT was obtained by reaction between QCD and montmorillonite suspensions, which could be attributed to the montmorillonite cation ion exchange properties. β-CD cavities of this composite were expected to capture organic molecules through inclusion, while montmorillonite units acted as the adsorption sites for metals. QCD-MMT was characterized by FT-IR, elemental analysis, XRD, SEM-EDX, and TGA. Adsorptions of Cr(VI), methyl orange, and p-nitrophenol were highly dependent on adsorbent dose, initial concentration, temperature, contact time, and pH. Adsorption kinetics of Cr(VI), methyl orange, and p-nitrophenol followed the pseudo-second-order model. Meanwhile, adsorption of Cr(VI) fit better in the Freundlich model, inferring a multilayer adsorption, while the adsorption of methyl orange and p-nitrophenol fit better in Langmuir model, inferring a monolayer adsorption. Thermodynamic analysis showed that the adsorptions were all endothermic process and could be spontaneous at given temperature range, except for Cr(VI), of which adsorption should be at much higher temperature. Overall, QCD-MMT exhibited potential for practical applications in the treatment of both metal ions and organic pollutants.

Keywords Beta-Cyclodextrin · Montmorillonite · Composite · Adsorption capacity

A. Zeng (✉) · A. Zeng
College of Light–Textile Engineering, Liming Vocational University, Quanzhou 362000, China
e-mail: anrongzeng@qq.com

A. Zeng · A. Zeng
Applied Technology Center of Fujian Provincial Higher Education for Practical Chemical Material, Quanzhou 362000, China

1 Introduction

With rapid development of industrialization and urbanization, a variety of hazardous molecules was used and could be possibly discharged into the natural environment. For example, synthetic dyes were commonly used in textile, cosmetics, and other industries (Yan et al. 2016). Dye containing wastewater could endanger human health without effective treatment. Also, pollutants like p-nitrophenol has become one of the commonly encountered pollutants in water pollution, and it could be persistent, bio-accumulative, and highly toxic at very low concentration (Shen et al. 2015). Moreover, metal-bearing effluents originating from metal plating, mining operations, nuclear power plant, and metallurgical and battery manufacturing industries, often contained many kinds of heavy metal ions, such as lead, cobalt, nickel, cadmium, chromium, and mercury ions. Heavy metals were non-biodegradable and can accumulate slowly in the body of living creatures, causing various diseases such as poisoning, nervous system damage, and cancer (Vašák and Meloni, 2011; Zheng 2001). Overall, those

pollutants could further lead to many serious environmental problems, like water pollution and further serious public health issue. Therefore, effective treatments are becoming more and more urgent.

A lot of water treatment methods have been reported. For example, adsorption, ion exchange, and reverse osmosis have been applied to the removal of chromium and mercury in paper and textile industries (Liu et al. 2016). Oxidation, membrane separation, and extraction were also developed to remove p-nitrophenol or its analogues from wastewater (Shen et al. 2015). For dyes containing wastewater treatment, methods like adsorption, oxidation process, precipitation, coagulation, and electro-chemical treatment could be applied (Debnath et al. 2017). Among these approaches, adsorption was used most frequently. It was cost saving, efficient, and promising to remove both organics and heavy metals from wastewater (Chen et al. 2015; Debnath et al. 2017). β-cyclodextrin (β-CD) has been found to be effective to remove heavy metals (Liu et al. 2016). It is usually used as a kind of pharmaceutical excipients. β-CD has a torus-shaped cyclic oligosaccharide structure with abundant hydroxyl groups on both ends, and a hydrophobic cavity. As a result, it shows good ability to capture organic molecules. However, the water-solubility of β-CD limits its application to some extent, and it is important to improve its insolubility in water. One way reported was to use cross-linkers to obtain β-CD polymers. For example, EDTA-β-CD was employed in the adsorption of aqueous dyes and metal ions (Zhao, Repo, Meng, et al., 2015b; Zhao, Repo, Yin, et al., 2015a). The enhanced metal adsorption ability of β-CD was attributed to EDTA's functional groups of chelating metal ions. Similar modifications were reported to improve the chitosan's metal ion affinities as well, by using EGTA, EDTA, and DTPA (Zhao, Repo, Sillanpää, et al., 2015c; Zhao et al. 2013). Another way to increase β-CD insolubility was to prepare inorganic-organic composite adsorbents, which has been applied to improve certain polymer's adsorption performance. For instance, hydroxamic-acid-modified polyacrylamide/Fe_3O_4 composite was prepared and showed affinity towards Cd(II), Pb(II), Co(II), and Ni(II) (Zhao et al. 2014).

Montmorillonite (MMT), with an ideal molecular formula of $[Al_2(Si_4O_{10})(OH)_2 \cdot XH_2O]$, is present in a type of hydrous, porous aluminum silicate layer mineral. MMT mines are abundant in nature, and their price is quite low. In terms of its cheapness and features (Li et al. 2014), it was widely used as an adsorbent for water treatment, especially for heavy metal treatment.

In this work, we prepared a β-CD/MMT composite (QCD-MMT) for adsorption of Cr(VI) ions (as the representative of heavy metal ions), methyl orange (as the representative of dye compounds), and p-nitrophenol (as the representative of phenols pollutants), in aqueous solution. In order to further investigate the interaction between QCD-MMT and different adsorbates, the adsorption behavior was studied in terms of various parameters such as adsorption kinetics, adsorption isotherms, and thermodynamic models.

2 Materials and Methods

2.1 Materials

β-CD was 96% pure and purchased from Aladdin. MMT was purchased from Zhejiang Fenghong New Material Co. Ltd., industrial grade; 2,3-epoxypropyltrimethyl ammonium chloride (EPTAC) was purchased from Shanghai Dibo Chemical Co. Ltd., analytical grade. Other reagents were purchased from Xilong Scientific, analytical grade. All reagents were used without further purification.

Potassium dichromate, methyl orange, and p-nitrophenol stock solutions were prepared via dissolving in deionized water. Working solutions of metals and dyes were prepared by diluting the stock solutions. The three adsorbates properties were summarized in Table 1.

2.2 Synthesis of QCD-MMT Composite

The synthetic process of QCD-MMT was shown in Fig. 1. β-CD was dissolved in NaOH solution (pH = 12) in a flask equipped with a mechanical stirrer, thermometer, reflux cooler, and drop funnel. EPTAC aqueous solution (75% by weight) was added into the drop funnel and further added dropwise into the flake. Mass ration of EPTAC and β-CD was 80/20. The reaction was conducted at 60 °C for 3 h. Then the reaction system was cooled to room temperature to obtain QCD.

MMT was suspended in water with QCD. Mass ratio of MMT and β-CD was of 10/1. The reaction was further conducted for another 24 h while sufficiently stirring at room temperature. The pH was adjusted to neutral with hydrochloric acid solution. The solid was

Table 1 Adsorbates used in this paper

Adsorbates	Chemical Formula
Potassium dichromate	$K_2Cr_2O_7$
Methyl orange	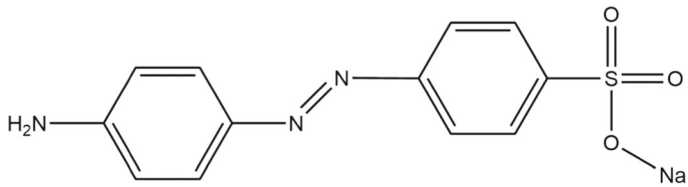
p-nitrophenol	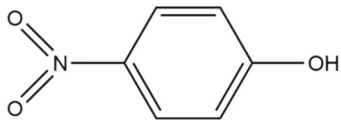

further purified with deionized water, followed by drying in a vacuum oven of 60 °C. The final product was QCD-MMT composite.

2.3 Characterization of QCD-MMT Composite

β-CD, MMT, and QCD-MMT FT-IR spectra were obtained using Bio-Rad FTS 6000 spectrometer. All samples were prepared as KBr pellets. Elemental analysis was determined using an Elementar Vario EL Cube analyzer, CHN mode. X-Ray diffraction (XRD) data of MMT and QCD-MMT power samples were performed with Bruker powder X-ray diffractometer D8 Advance, with scan range from 5° to 90° (2θ). The surface morphology and energy-dispersive X-ray (EDX) spectroscopy were performed by field emission scanning electron microscopy (FE-SEM, Hitachi S4800). Thermogravimetric analysis (TGA) was also conducted on a TA instrument Q500 to assess QCD-MMT's thermal stability and organic content. Samples were heated to 800 °C at a heating rate of 10 °C/min in a nitrogen flow of 40 ml/min.

The organic content was calculated as the percentage of organic mass with respect to the dried mass of MMT. The dried mass of initial mass was obtained at 200 °C from thermogravimetric curves in order to avoid the contribution of water, which could introduce error if samples were not dried correctly. The mass of organic compounds was calculated from the mass loss registered between 200 and 800 °C, so the organic content would be calculated as following Eq. (1) (Ezquerro et al. 2015):

$$\text{Orangic content} = \left(\frac{m_i - m_f}{m_i} \times 100\right) - \%\Delta m_{\text{MMT}} \quad (1)$$

where m_i and m_f were the mass of QCD-MMT at 200 and 800 °C, respectively; $\%\Delta m_{\text{MMT}}$ was the mass loss

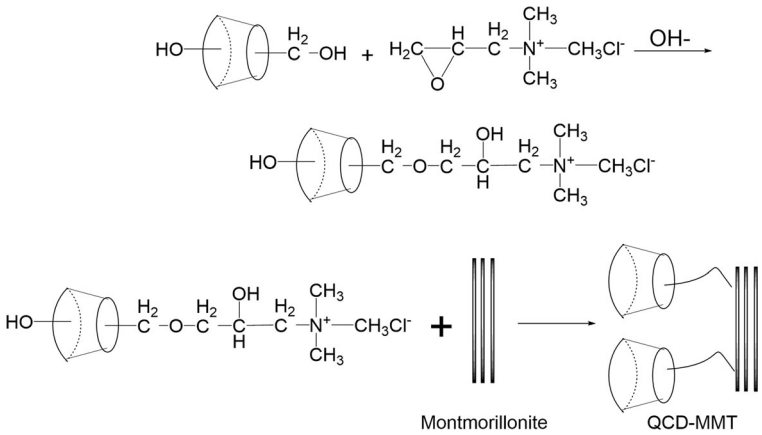

Fig. 1 Synthesis of QCD-MMT composite

observed in the same region of temperature for the unmodified sample. The decomposition of organics took place in the range of 200 to 500 °C. The final temperature was chosen at 800 °C, since some overlap with the dihydroxylation of silicate layers was observed at around 500 °C.

The ratio of quaternary ammonium groups of QCD-MMT was determined by N element ratio from element analysis, compared with the results of Cl element percentage from EDX.

2.4 Adsorption Experiments

2.4.1 Adsorption Parameters' Impact on QCD-MMT's Adsorption Performance

All adsorption experiments were undertaken by mixing adsorbents with 30 mL potassium dichromate, methyl orange, and p-nitrophenol solutions of different initial mass concentrations. The impacts of usage, initial concentration, temperature, contact time, and pH were determined.

For each adsorption system, the residual in the reaction mixture was analyzed by centrifuging the reaction mixture, and then measuring the absorbance of the supernatant at the wavelength corresponding to the maximum absorbance of the sample. Concentrations in the reaction mixture were calculated from the calibration curve. Methyl orange and p-nitrophenol concentrations were determined by UV-vis spectrometry (T6 model, Beijing Purkinje General Instrument Co., Ltd.) at the maximum absorbance of dyes. Metal concentrations were analyzed by an atomic absorption spectroscopy (A3 model, Beijing Purkinje General Instrument Co., Ltd.).

The amount of adsorbate adsorbed onto QCD-MMT, q_e (mg/g), was calculated by the following mass balance relationship:

$$q_e = (C_0 - C_e)\frac{V}{W} \tag{2}$$

where C_0 and C_e were initial and equilibrium liquid-phase concentration of waste, respectively (mg/L), V was the volume of the solution (L), and W was the weight of the QCD-MMT used (g).

2.4.2 Adsorption Kinetics Analysis

To determine QCD-MMT's adsorption kinetics of Cr(VI), methyl orange and p-nitrophenol, independent bottles containing 30 mL samples and 0.05 g QCD-MMT, were used to get accurate results for each point on the graph. The initial concentration of potassium dichromate solution, methyl orange solution and p-nitrophenol solution was 360, 250, and 25 mg/L, respectively. Adsorption experiments' contact time varied from 15 to 180 min. Adsorption was carried out at the temperature of 30 °C.

In order to investigate the adsorption mechanism of three different adsorbates, two commonly used reaction kinetic models viz., pseudo-first-order and pseudo-second-order models were used (Xing and Wang 2016). The kinetic data were utilized to investigate the suitability of these models. The linear equations of pseudo-first-order and pseudo-second-order models were expressed as Eqs. (3) and (4), respectively:

$$q_t = q_{e1} - q_{e1}e^{-k_1 t} \tag{3}$$

$$\frac{t}{q_t} = \frac{t}{q_e} + \frac{1}{k_2 {q_e}^2} \tag{4}$$

In Eq. (3), q_{e1} and q_t were the adsorption capacity at equilibrium and at time t, respectively (mg/g); k_1 was the rate constant of pseudo-first-order model (min^{-1}). In Eq. (4), q_{e2} and q_t were the adsorption capacity at equilibrium and at time t; k_2 (slope^2/intercept) was the pseudo-second-order rate constant (g/mg/min).

2.4.3 Adsorption Isotherms Analysis

Isothermal studies were conducted with QCD-MMT usage of 0.05 g and 30 mL adsorbates solutions by shaking the reaction mixture for equilibrium time. The adsorption temperature was of 303.15, 313.15, and 323.15 K, respectively.

The Langmuir model is valid for monolayer adsorption onto a surface with a finite number of identical sites. The Langmuir equation was as follows (Xing and Wang, 2016):

$$q_e = \frac{q_m K_L C_e}{1 + K_L C_e} \tag{5}$$

where C_e and q_e were equilibrium concentration (mg/L)

and the amount of adsorbates adsorbed on QCD-MMT (mg/g), respectively. The constant K_L was related to the energy of adsorption and the constant q_m represents the maximum amount of adsorbates absorbed per unit weight of QCD-MMT.

The Freundlich model can be applied to non-ideal sorption on heterogeneous surfaces as well as multilayer sorption and was expressed by the following equation (Xing and Wang, 2016):

$$q_e = K_F C_e^{\frac{1}{n}} \quad (6)$$

where K_F and n were the Freundlich constants. K_F and n are indicators of adsorption capacity and adsorption intensity of the QCD-MMT, respectively.

2.4.4 Adsorption Thermodynamics Analysis

The thermodynamic parameters (ΔH^0, ΔS^0, and ΔG^0) for three different adsorbates onto QCD-MMT can be calculated from the temperature-dependent adsorption isotherms. The equation was as follows (Li et al. 2013; Xing and Wang, 2016):

$$\ln K_0 = \frac{\Delta S^0}{R} - \frac{\Delta H^0}{RT} \quad (7)$$

where R is the universal gas constant (8.314 kJ/(mol K)); T is the temperature in Kelvin; K_0 is the adsorption equilibrium constant and can be calculated by plotting ln K_d versus C_e and extrapolating C_e to zero, where K_d was defined as q_e divided by C_e.

3 Results and Discussion

3.1 Characterizations of QCD-MMT

3.1.1 FT-IR Spectroscopy

Figure 2 showed the FT-IR spectra of raw β-CD, raw MMT, and QCD-MMT composite. Compared with MMT, the peaks at 2928 cm^{-1} of QCD-MMT could be attributed to the methyl groups' asymmetric stretching vibration (Zhao et al. 2009). The peaks at 1487 cm^{-1} of QCD-MMT indicated the existence of $-CH_2$-N^+, compared to β-CD, and could be assigned to NH_3^+. Besides, a characteristic absorption peak of α-type glycosidic bond was found at 855 cm^{-1} of QCD-MMT, which indicates that β-CD was formed by glucopyranose units through α-1,4-glycosidic bond (Yuan et al. 2015). The peak of 1414 cm^{-1} was one of the typical peaks corresponding to the deformation vibration of the O-H bonds in the primary and secondary hydroxy groups of β-CD, and also C-H bending vibrations (Zhao et al. 2009). It could be inferred that the structure characteristics of β-CD were maintained. Moreover, compared MMT with QCD-MMT, the peaks at 521 and 465 cm^{-1} could be attributed to the Si-O-Al stretching vibration and Si-O bending vibration. Therefore, it could be concluded that the modification of β-CD and MMT was successful.

3.1.2 Element Analysis

The results of quantitative elemental analysis were presented in Table 2. Data showed the C and N element content of QCD-MMT was increased. The calculated quaternary ammonium group percentage was 8.22 wt.% basing on N element content. This proved the final product was quaternized successfully. This inference was echoed by EDX. EDX-Cl element content was also given in Table 2, and the calculated quaternary ammonium group percentage was 13.02 wt.%. EDX spectrum was recorded to identify the expected compositions on a selected rectangle area of MMT and QCD-MMT sediment. The difference between two results might be explained by uneven quaternary ammonium group distribution. There might be more quaternary ammonium groups on QCD-MMT's surface. In this paper, results based on element analysis were determined as the quaternary ammonium group percentages.

3.1.3 X ray Diffraction (XRD)

Figure 3 displayed the XRD pattern of raw MMT and QCD-MMT. It showed that raw MMT has a d (001)-spacing of 1.335 nm, basing on Bragg Eq. (2)$d_{001}\sin\theta = \lambda$ (λ = 0.154 nm) calculation. After modification, the QCD-MMT's d_{001}-spacing was enlarged to 1.409 nm. It could be inferred that the modification may occur in the MMT interlayer. This might also benefit QCD-MMT's adsorption capacity.

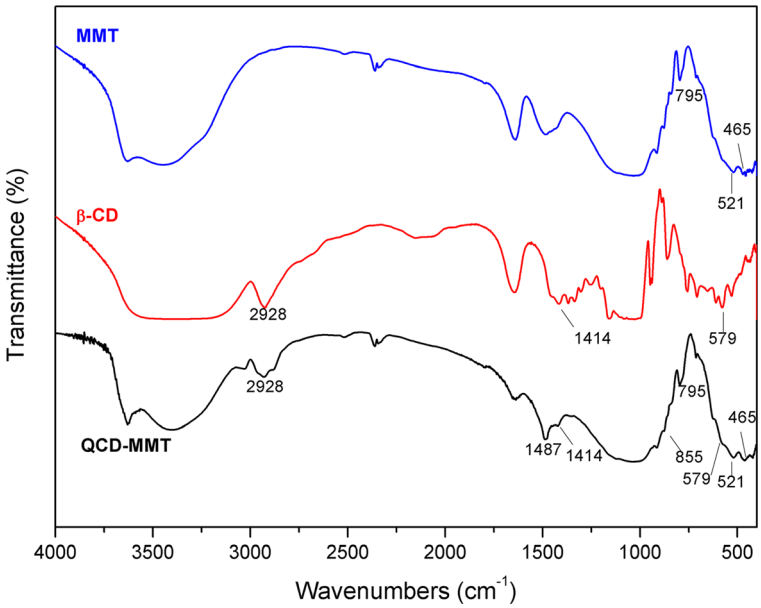

Fig. 2 FT-IR spectra of MMT, β-CD, and QCD-MMT

3.1.4 SEM-EDX Analysis

SEM provided information about morphology changes before and after modification. Images were collected in Fig. 4a, b. In the pristine state, MMT showed a rough surface where large lamellas were observed. QCD-MMT's surface was smooth after modifications with QCD.

Simultaneously to SEM images, EDX spectroscopy analysis was also carried out to determine the quaternary ammonium amount. Results were shown in Fig. 5 and Table 3. Cl element content was increased from 0.09 wt.% to 3.14 wt.%. Cl ion was the counter ion of quaternary ammonium in QCD-MMT and indicated that the MMT had been quaternized successfully (Rosa et al. 2008; Sowmya and Meenakshi, 2013; Yao et al. 2014). However, since EDX only analyzes the surface and identify the expected composition on a selected rectangle area, we took EDX as supplement data for element analysis.

3.1.5 Thermogravimetric Analysis

TGA and derivative thermogravimetric (DTG) curves were shown in Figs. 6 and 7, respectively, and were also summarized in Table 4. The DTG curves provided information about different steps of decompositions. The thermal decomposition of MMT could be divided into four different regions (Ezquerro et al. 2015; Xie et al. 2014). The first weight loss region was desorption of water and physisorbed species, which happened below 180 °C. The second region was located in the range from 200 to 500 °C and involves the decomposition of organic species. The third region

Table 2 MMT and QCD-MMT element analysis

Sample	Element content (wt.%)			Total quaternary ammonium group wt.%	Quaternary ammonium group wt.% (EDX result)
	N	C	H		
MMT	0.56	0.95	1.827	/	/
QCD-MMT	1.32	11.19	2.709	8.22[a]	13.02[b]

[a] Calculated from nitrogen content of element analysis: quaternary ammonium group wt.% = (1.32–0.56)/M_N * M_{EPTAC}, where M_N stands for molar mass of N element, M_{EPTAC} stands for molar mass of EPTAC

[b] Calculated from chlorine content of EDX analysis: quaternary ammonium group wt.% = (3.14–0.09)/M_{Cl} * $M_{EPTAC,xxx}$ where M_{Cl} stands for molar mass of Cl element, M_{EPTAC} stands for molar mass of EPTAC

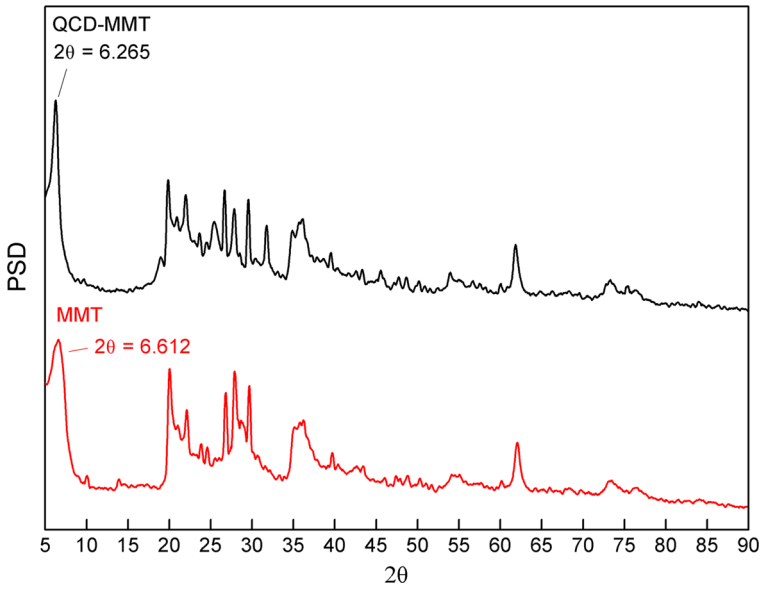

Fig. 3 XRD patterns of MMT and QCD-MMT

was from 500 to 700 °C, when aluminosilicate layers' dehydroxylation took place. Finally, in the last step between 700 and 1000 °C, the evolution of products associated with organic carbonaceous residue occurs.

The position of these steps in the derivative mass curves is referred as the temperature of maximum decomposition rate in Table 4 (T_1, T_2, and T_3). T_1 corresponds to desorption of water and other physisorbed species, T_2 refers to the decomposition step of organic species, and T_3 refers to the aluminosilicate layers' dihydroxylation. The decomposition of carbonaceous residue was not registered in the curves below the maximum tested temperature of 800 °C.

DTG of MMT showed only two peaks (T_1 and T_3). The first one was below 100 °C (T_1), and the mass loss was associated to the evaporation of water adsorbed. The second decomposition step occurred in the range 550–750 °C (T_3) and could be attributed to the dihydroxylation of the layer crystal lattice. QCD-MMT showed one additional peak at around 304 °C, which was associated to the decomposition of organic compound introduced to MMT.

Organic content of QCD-MMT was calculated basing on TGA result, which was 16.25 wt.%. Considering element analysis results, CD content was around 8.03 wt.%, while QCD content was around 9.10 wt%. Those results were also given in Table 4.

3.2 Cr(VI), Methyl Orange and p-Nitrophenol Adsorption Experiments

3.2.1 Influence of QCD-MMT Usage

The influence of adsorbent usage was studied, and the results were shown in Fig. 8, where q_e represented the sorption amount of Cr(VI), methyl orange and p-nitrophenol on QCD-MMT (mg/g) in equilibrium time. At the usage of 0.05 g, the adsorption capacity for Cr(VI), methyl orange, and p-nitrophenol was 51.98, 25.00, and 24.56 mg/g, respectively. Adding more adsorbent will decrease the adsorption capacity. It could be also noticed that the difference between initial concentration and C_e did not fluctuate a lot (C_e values of Cr(VI), methyl orange, and p-nitrophenol shown in Fig. 8). This could be explained by that the adsorption was driven by adsorbates' concentration gradient (Xing and Wang, 2016). Given that concentration gradients in each adsorption were similar and the total adsorbates adsorbed did not change a lot, the adsorption capacity would be decreased when QCD-MMT usage increased. Also, the aggregation and competition of QCD-MMT adsorbent might also have impacts the adsorption behaviors.

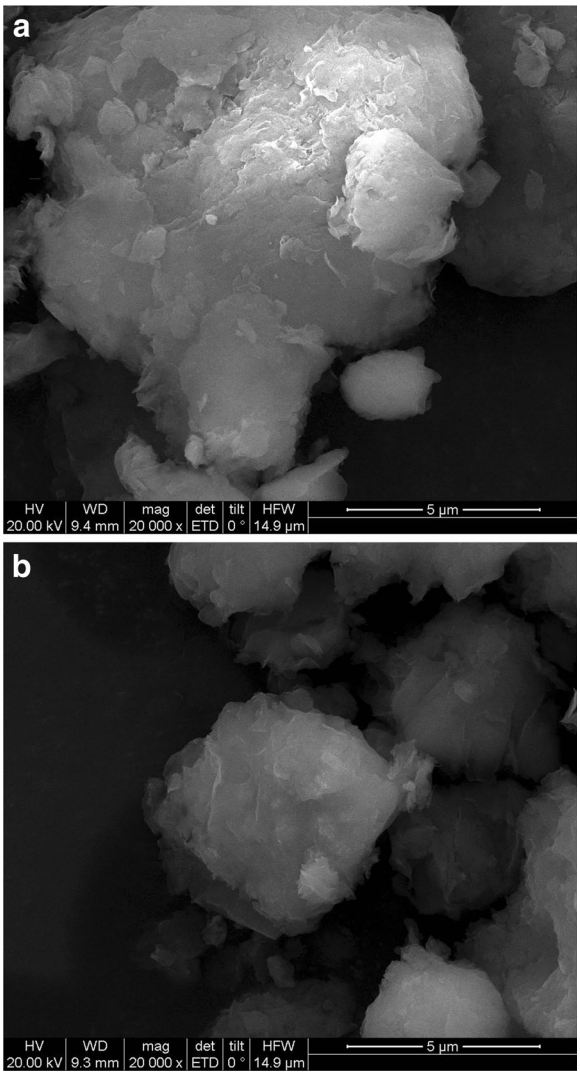

Fig. 4 SEM images of MMT (**a**) and QCD-MMT (**b**)

3.2.2 Influence of Initial Concentration

Figure 9 showed the influence of the initial concentrations on QCD-MMT's sorption levels, respectively. The adsorption capacities of Cr(VI) increased as the initial concentrations increased. Methyl orange and p-nitrophenol showed similar trends. When the initial methyl orange concentration was up to 250 mg/L at different temperatures of 30, 40 and 50 °C, the adsorption capacity was 53.217, 58.784, and 64.881 mg/g, respectively. For p-nitrophenol, when the initial concentration was increased, the adsorption capacity was largely enhanced. The maximum adsorption was 51.212 mg/g at 50 °C, of which initial concentration was 200 mg/L. The increasing initial p-nitrophenol concentrations could not always increase adsorption. On the contrary, the adsorption was slightly lower. It was possible that high concentrations resulted in competition between p-nitrophenol and then slowed down the adsorption. Also, high concentration of p-nitrophenol might occupy and block the QCD-MMT inclusion sites at the surface, preventing further p-nitrophenol dispersion.

3.2.3 Influence of Contact Time

In order to determine the adsorption equilibration time of different adsorbates and also to investigate the kinetics of adsorption process, the adsorption capacity as a function of contact time was studied.

Three different samples showed similar trends. As adsorption time changed from 15 to 180 min, the adsorption capacity first increased steadily then afterwards no significant change observed. For Cr(VI) and methyl orange, near equilibrium was achieved in around 1.5 h, while for p-nitrophenol in around 2.5 h. This was probably due to larger surface area of QCD-MMT being available at the beginning for adsorptions. As time progressed, the surface coverage of the adsorbent was high and then no adsorption took place. Figure 10a–c showed the effect of time on adsorption. The equilibrium adsorption capacities of Cr(VI), methyl orange, and p-nitrophenol were around 43, 50, and 6.5 mg/g, respectively.

3.2.4 Influence of pH

Impact of pH was shown in Fig. 11. The adsorption capacities of Cr(VI) at different pH environment ranged from 34.80 to 51.98 mg/g. The adsorption capacities were higher at acidic and neutral condition. Maximum adsorption capacity of Cr(VI) reached the maximum at pH of 7. At lower pH, $HCrO_4^-$ was the major form of Cr(VI). It is possible that the quaternary ammonium groups on the adsorbents were easily protonated and positively charged, which facilitated the approach of the negatively charged $HCrO_4^-$ due to the electrostatic interaction (Liu et al. 2016). Also, at lower pH, the counter anion Cl^- of quaternary ammonium groups might be displaced by $HCrO_4^-$ (Wang

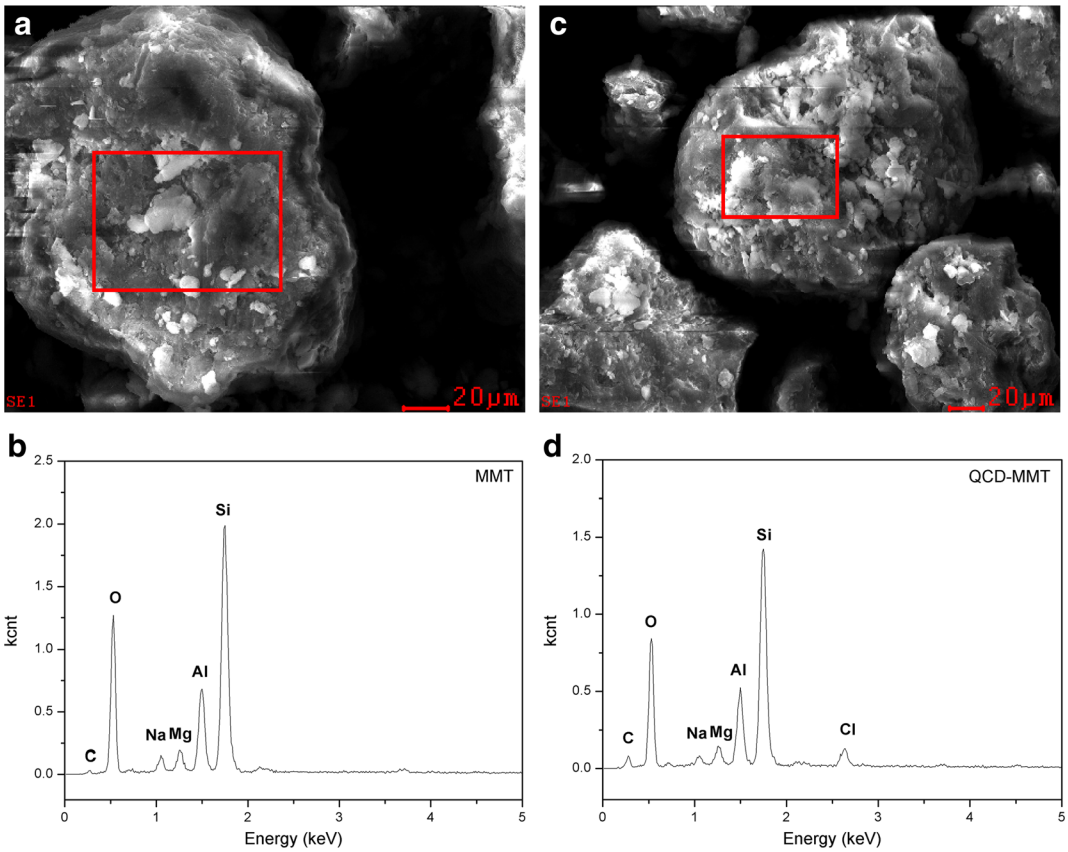

Fig. 5 SEM-EDX spectrum of MMT (**a**, **b**) and QCD-MMT (**c**, **d**) sediments

et al. 2016). Moreover, a probable mechanism was proposed to be ion exchange between chromium and surface −OH groups or hydroxide groups of Al polycations proceeded in the interlayer spaces. At lower pH, −OH groups were protonized to $-OH_2^+$, which facilitates the ligand exchange since $-OH_2^+$ is easier to displace from metal binding sites than −OH. The ion exchange could take place through the following reactions (Wang et al. 2016):

$$\equiv S-OH^- + H^+ \rightarrow \equiv S-OH_2^+$$

$$\equiv S-OH^- + HCrO_4^- \rightarrow \equiv S-HCrO_4^- + OH^-$$

$$\equiv S-OH_2^+ + HCrO_4^- \rightarrow \equiv S-HCrO_4^- + H_2O$$

Table 3 Composition of MMT and QCD-MMT determined by SEM-EDX

Element	MMT		QCD-MMT	
	Wt.%	At.%	Wt.%	At.%
CK	02.69	04.73	10.27	17.23
OK	39.16	51.67	36.19	45.58
NaK	02.70	02.48	01.66	01.45
MgK	02.91	02.53	02.39	01.98
AlK	10.98	08.59	09.26	06.92
SiK	35.72	26.85	30.48	21.86
ClK	00.09	00.05	03.14	01.78

For methyl orange, the adsorption capacities changed from 12.43 to 23.72 mg/g at different pH values. With pH value of 3 ~ 11, the adsorption capacities were around 22 mg/g without significant changes. The hydroxyl of QCD-MMT might form hydrogen bonds with N atoms of methyl orange skeleton. Meanwhile, hydroxyl proton can produce electrostatic adsorption with SO^{3-} contained in MO molecules (Yan et al. 2016). Moreover, the inclusion

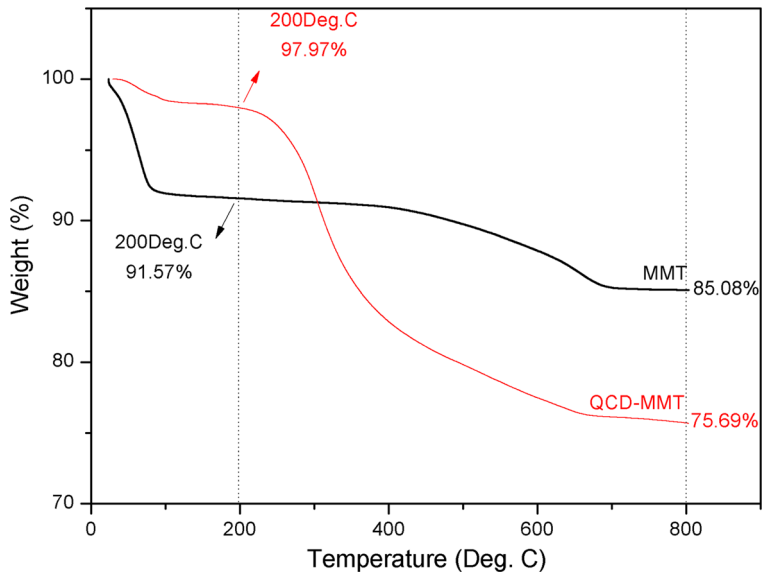

Fig. 6 TGA curves of MMT and QCD-MMT

between methyl orange and β-CD unit of QCD-MMT also benefit adsorption. When pH was of 13, the hydrogen bonds might not be easy to form between β-CD unit and methyl orange, since the OH^- in the solution would compete with methyl orange and form hydrogen bonds with β-CD unit. This would further decrease electrostatic adsorption and then inclusion, resulting in lower adsorption (Yan et al. 2016).

For p-nitrophenol, the maximum adsorption was obtained at pH of 5, which was 21.45 mg/g. Also, at pH of 11, the adsorption was high (19.36 mg/g) as well. The fluctuation could be explained by the combination of host-guest inclusion, electrostatic repulsion, and hydrogen bond interaction (Li et al. 2011; Shen et al. 2015). When pH was low, both β-CD unit and p-nitrophenol become protonated, so p-nitrophenol cannot be adsorbed on β-CD efficiently for the electrostatic repulsion between them. This results in lower adsorption capacity at pH of 1 and 3. When pH value increased, protonation of β-CD and p-nitrophenol became weak. This might benefit the host-guest inclusion between them, and reach the maximum adsorption at pH of 5. As the pH became higher (pHs of 7 and 9), inclining adsorption was

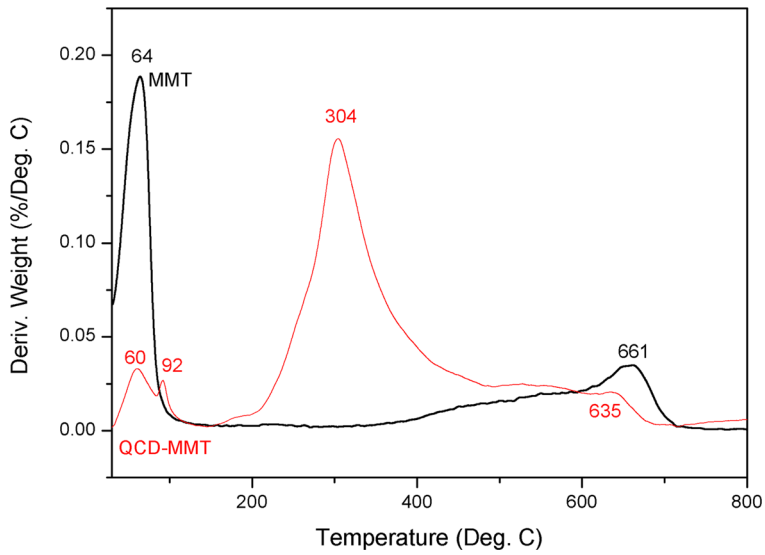

Fig. 7 DTA curves of MMT and QCD-MMT

Table 4 TGA-DTG results of MMT and QCD-MMT

Sample	Temperature of maximum decomposition rate (°C)			Residue at 800 °C (wt.%)	Organic content (wt.%)	CD content (wt.%)	QCD content (wt.%)	Total EPTAC content (wt.%)
	T_1	T_2	T_3					
MMT	64	–	661	85.08	/	/	/	/
QCD-MMT	60 92	304	635	75.69	16.25[a]	8.03[b]	9.10[b]	8.22[b]

[a] Organic content calculated from Eq. (1)

[b] CD content calculated from following equations:

$M_{QCD} * n_{QCD} + M_{EPTAC} * n_{EPTAC}$ = organic content

$n_{QCD} + n_{EPTAC} = m_N / M_N$

$n_{QCD} = n_{CD}$

where M_{QCD} stands for molar mass of QCD, M_{EPTAC} stands for molar mass of EPTAC, n_{QCD} stands for mole number of QCD, n_{EPTAC} stands for mole number of EPTAC, m_N stands for mass of N element, and M_N stands for molar mass of N element

observe. When the pH reached pH of 11, the alkaline environment greatly weakened the protonation of β-CD and p-nitrophenol, so the increased adsorption capacity could be attributed to host-guest inclusion and hydrogen bond interaction. However, when the pH was of 13, certain amount

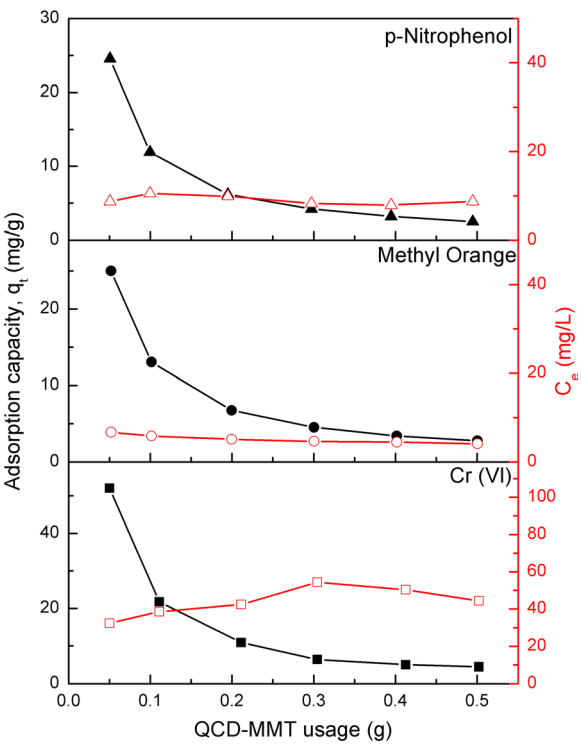

Fig. 8 Influence of usage on QCD-MMT adsorption capacity and adsorbates' equilibrium concentration (contact time 24 h; initial concentration Cr(VI) 120 mg/L, methyl orange 50 mg/L, p-nitrophenol 50 mg/L; temperature 30 °C; neutral)

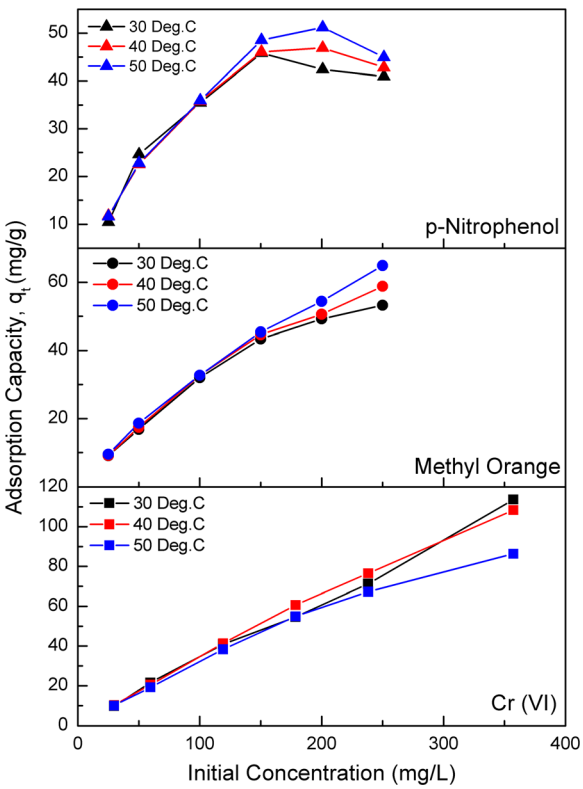

Fig. 9 Influence of adsorbates' initial concentrations on adsorption capacity on different temperatures (contact time 24 h; QCD-MMT usage 0.05 g; neutral)

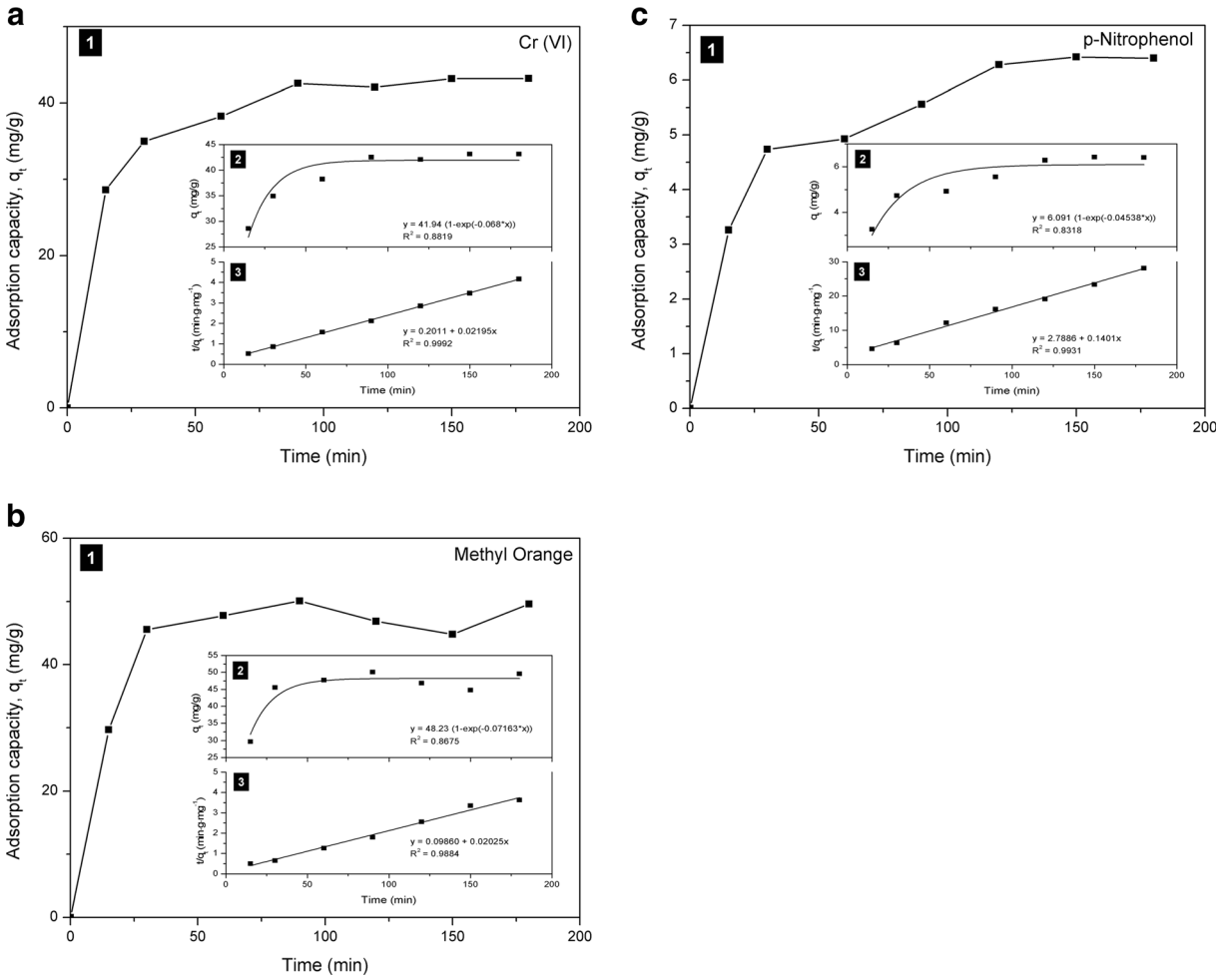

Fig. 10 *1* QCD-MMT's adsorption capacity was plotted as a function of time. Adsorption kinetics was investigated using *2* pseudo-first-order and *3* pseudo-second-order models. **a** Cr(VI), QCD-MMT 0.05 g, 30 °C, neutral, initial concentration 120 mg/L. **b** Methyl orange, QCD-MMT 0.05 g, 30 °C, neutral, initial concentration 250 mg/L. **c** p-Nitrophenol, QCD-MMT 0.05 g, 30 °C, neutral, initial concentration 25 mg/L

of p-nitrophenol might form p-nitrophenol sodium salt with sodium hydroxide. The hydrophobic inclusion could be impacted, causing decreasing adsorption.

Overall, the adsorption was pH dependent. More investigation would be conducted in the future to explore more details about the mechanism.

3.3 Adsorption Kinetics

Pseudo-first-order and pseudo-second-order models were used to evaluate the sorption kinetic. The kinetic parameters for adsorption of three different samples were given in Table 5. For all three samples, the pseudo-second-order equation fitted better for the data, considering higher R^2 and higher agreement between the calculated and experimental q_e values. This explained chemisorption controls the rate of adsorption. Table 5 and Fig. 12 showed the detailed values. In chemisorption, the adsorbate adhered on QCD-MMT by formation of a chemical bond, and also searched for adsorption sites. This would maximize their coordination number with the surface (Kumar and Kirthika, 2009; Mishra et al. 2017). Furthermore, the kinetics of p-nitrophenol and methyl orange was faster than that of Cr(VI), suggesting that the β-CD cavities inclusion process was faster than MMT complexing, comparing pseudo-second-order rate constant k_2 values (Zhao, Repo, Yin, et al., 2015a).

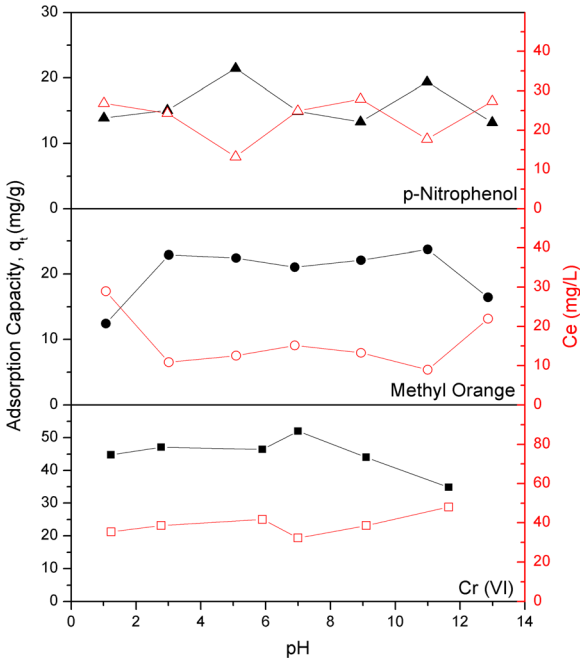

Fig. 11 Influence of pH on QCD-MMT adsorption capacity and adsorbates' equilibrium concentration (contact time 24 h; initial concentration Cr(VI) 120 mg/L, methyl orange 50 mg/L, p-nitrophenol 50 mg/L; temperature 30 °C; neutral)

3.4 Adsorption Isotherms

As shown in Fig. 12 and Table 6, the Langmuir isotherm model provides the better fit for the methyl orange and p-nitrophenol equilibrium data. This suggested that the adsorption for methyl orange and p-nitrophenol was monolayer, or homogeneous adsorption (Debnath et al. 2017). Each methyl orange or p-nitrophenol molecule might have equal adsorption affinity towards QCD-MMT (Shen et al. 2015). It was possible that the monolayer coverage of methyl orange or p-nitrophenol molecule was formed at the outer surface of QCD-MMT (Malik 2004). Since β-CD was the effective component for organic methyl orange and p-nitrophenol, it would be inferred that the β-CD distributed homogenously at the final QCD-MMT composite. Debnath et al. reported the similar observation (Debnath et al. 2017). They used β-CD modified pinecone to remove safranine O, brilliant green, and methylene blue; the adsorption also followed the Langmuir isotherm.

The introduction of β-CD to the QCD-MMT composite enabled the cavity structure to capture organic molecules. It may be inferred that the interactions between the organic molecules used in this article and the β-CD were primarily due to host-guest inclusion. Also, methyl orange and p-nitrophenol molecules might have possible hydrogen bonding with the hydroxyl groups on the surface of the β-CD.

Cr(VI) adsorption fits Freundlich isotherm model better, suggesting a multilayer adsorption for Cr(VI). This result could be attributable to the large montmorillonite spacing and the cationic adsorption sites for Cr(VI) due to surfactant loadings. These cationic adsorption sites might be favorable to the Cr(VI) adsorption through anion exchange between the counter anion of surfactant and $HCrO_4^-$ or $Cr_2O_7^{2-}$ (Wang et al. 2016). The Cr(VI) adsorption on QCD-MMT might also depended on electrostatic attraction and the ion exchange between chromium and surface −OH groups (Li et al. 2014). Also, the value of n from Freundlich isotherm model was found to be slightly higher than 1, which means that the adsorption for Cr(VI) was a linear sorption.

Table 5 Adsorption kinetics of methyl orange on QCD-MMT

Kinetic models	Equation	Adsorbates	Parameters			
			k	Experimental q_e (mg/g)	Calculated q_e (mg/g)	R^2
Pseudo-first order	$q_t = q_{e1} - q_{e1} e^{-k_1 t}$	Cr(VI)	0.068	43.000	41.943	0.8819
		Methyl orange	0.072	50.000	48.227	0.8675
		p-Nitrophenol	0.045	6.500	6.091	0.8318
Pseudo-second order	$\frac{t}{q_t} = \frac{t}{q_{e2}} + \frac{1}{k_2 q_{e2}^2}$	Cr(VI)	0.002	43.000	45.558	0.9992
		Methyl orange	0.004	50.000	49.383	0.9884
		p-Nitrophenol	0.007	6.500	7.136	0.9931

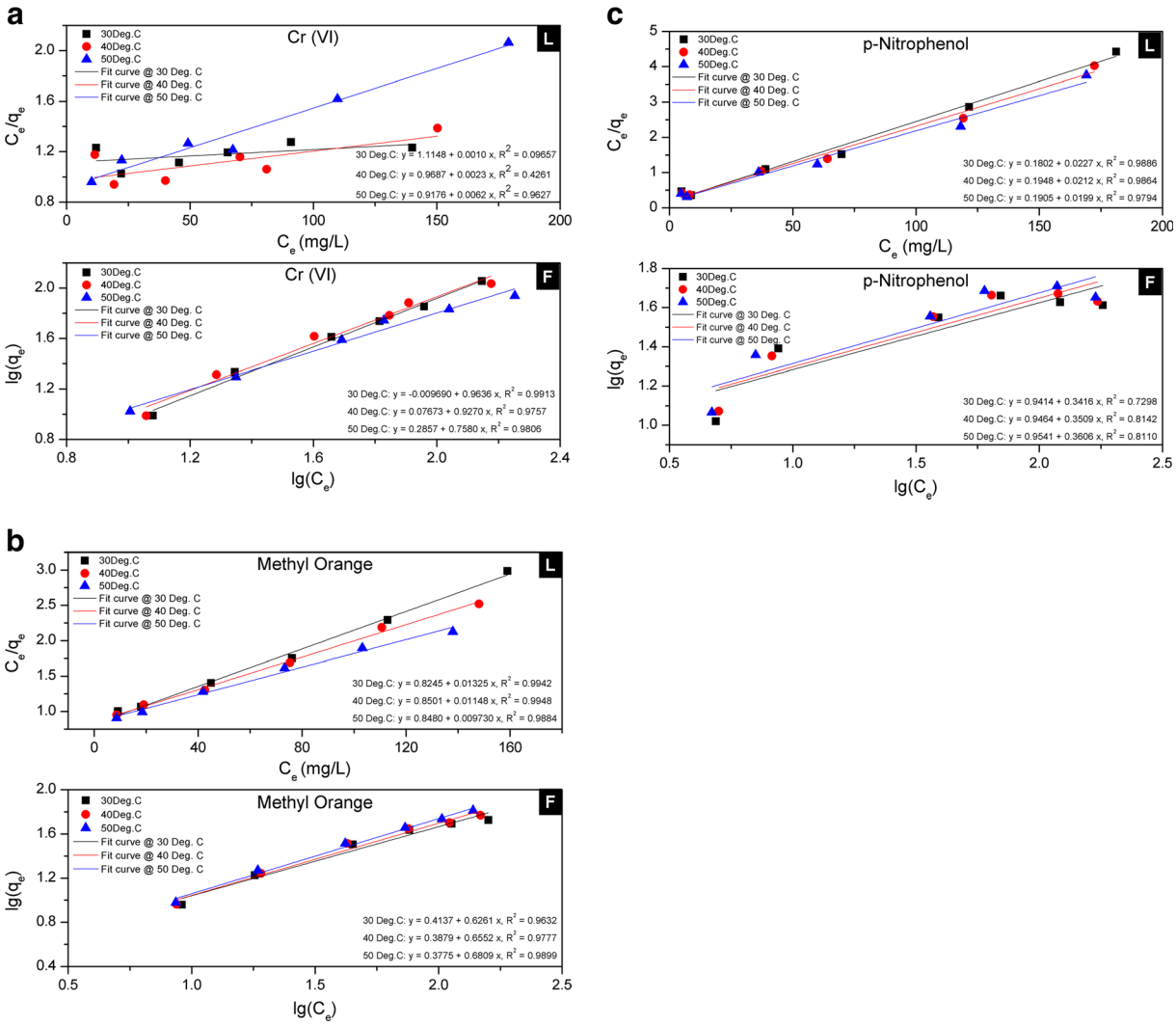

Fig. 12 Adsorption isotherm on QCD-MMT using *L* Langmuir and *F* Freundlich isotherm model. (The *solid line* represented the fit curves. Neutral solutions; QCD-MMT usage of 0.05 g; contact time of 24 h **a** Cr(VI); **b** methyl orange; **c** p-nitrophenol)

3.5 Adsorption Thermodynamics

As shown in Table 7, for all three adsorbates, the positive standard enthalpy change ΔH^0 values indicated that the adsorption was endothermic process. The negative standard free energy change ΔG^0 values and positive standard entropy change ΔS^0 values indicated that the adsorption process was spontaneous with high affinity. ΔG^0 values decreased with the increasing temperature, implying more efficient adsorption at higher temperatures. For Cr(VI) adsorption, the ΔG^0 values became negative when temperature was higher, around 50 °C.

4 Conclusions

In this paper, the adsorption capacities of QCD-MMT composite towards Cr(VI), methyl orange, and p-nitrophenol were studied. The adsorption capacities might be attributed both to the hydrophobic cavity of β-CD and the special metal-removing capacities of MMT.

β-CD was cyclic oligosaccharides including glucose units linked by α-1,4-glucosidic bonds (Zhang et al. 2013), which has a hydrophobic inner cavity and a hydrophilic exterior (Qiao et al. 2010). This special

Table 6 Isotherm parameter for adsorption of Cr(VI), methyl orange, and p-nitrophenol on QCD-MMT

	Temperature	Langmuir			Freundlich		
	K	R^2	q_{max} mg/g	K_L L/mg	R^2	K_F (mg/g)(mg/L)^n	n
Cr(VI)	303.15	0.096	980.39	0.001	0.991	0.98	1.038
	313.15	0.426	423.73	0.002	0.976	1.19	1.079
	323.15	0.963	159.24	0.007	0.981	1.93	1.319
Methyl orange	303.15	0.994	75.47	0.016	0.963	2.59	1.597
	313.15	0.995	87.11	0.866	0.978	2.44	1.526
	323.15	0.988	102.77	0.011	0.99	2.39	1.468
p-Nitrophenol	303.15	0.988	44.05	0.126	0.73	8.74	2.927
	313.15	0.986	47.12	0.109	0.814	8.84	2.849
	323.15	0.979	50.15	0.105	0.811	9.00	2.773

cavity structure of β-CD constituted a kind of non-polar micro-environment, allowing a number of small object organic molecules and inorganic ions to enter. It could package multiple object molecules to form supramolecular complexes. The adsorption of methyl orange and p-nitrophenol in this study could be ascribed to the inclusion in the hydrophobic cavity of β-CD and hydrogen bond interaction (Badruddoza et al. 2013; Shen et al. 2015). The kinetics study also showed that p-nitrophenol and methyl orange adsorption followed pseudo-second-order model and was faster than that of Cr(VI), suggesting that the β-CD cavities inclusion process was faster than MMT complexing (Zhao, Repo, Yin, et al., 2015a). Moreover, the isotherms fitting results of methyl orange and p-nitrophenol adsorption indicated that the absorption of these two molecules were better described by Langmuir model, which was monolayer, or homogeneous.

The composite also utilized MMT's significant adsorption capacities towards metal ions. This study used Cr(VI) as a representative. The adsorption of Cr(VI) was highly dependent on adsorbent dose, initial concentration, temperature, and contact time. The adsorption kinetics of QCD-MMT followed the pseudo-second-order model. Adsorption of Cr(VI) also fits better in the Freundlich model, inferring a multilayer adsorption.

Thermodynamic analysis showed that the adsorption was all endothermic process and could be spontaneous at given temperature range, except for Cr(VI), of which adsorption should be at much higher temperature.

Further studies would be focused more on the adsorption towards mixed wastewater containing different types of pollutants. More detailed investigation into adsorption mechanism would be conducted as well.

Table 7 Thermodynamic parameters of Cr(VI), methyl orange, and p-nitrophenol adsorption

Adsorbates	ΔH^0, kJ/mol	ΔS^0, J/(mol k)	ΔG^0, kJ/mol 303.16 K	ΔG^0, kJ/mol 313.16 K	ΔG^0, kJ/mol 323.16 K
Cr(VI)	5.38	17.03	0.22	0.05	−0.12
Methyl orange	2.48	8.43	−0.08	−0.16	−0.24
p-Nitrophenol	4.71	21.83	−1.90	−2.12	−2.34

Acknowledgements The Science Foundations from the Department of Education, Fujian Province (JA14428) and from Liming Vocation University (LZ2016109) were acknowledged.

References

Badruddoza, A. Z. M., Shawon, Z. B. Z., Wei, J. D. T., Hidajat, K., & Uddin, M. S. (2013). Fe_3O_4/cyclodextrin polymer nanocomposites for selective heavy metals removal from industrial wastewater. *Carbohydrate Polymers, 91*(1), 322–332.

Chen, J., Qiu, F., Xu, W., Cao, S., & Zhu, H. (2015). Recent progress in enhancing photocatalytic efficiency of TiO_2-based materials. *Applied Catalysis A General, 495*, 131–140.

Debnath, S., Ballav, N., Maity, A., & Pillay, K. (2017). Competitive adsorption of ternary dye mixture using pine cone powder modified with β-cyclodextrin. *Journal of Molecular Liquids, 225*, 679–688.

Ezquerro, C. S., Ric, G. I., Miñana, C. C., & Bermejo, J. S. (2015). Characterization of montmorillonites modified with organic divalent phosphonium cations. *Applied Clay Science, 111*, 1–9.

Kumar, P. S., & Kirthika, K. (2009). Equilibrium and kinetic study of adsorption of nickel from aqueous solution onto bael tree leaf powder. *Journal of Engineering Science & Technology, 4*(4), 351–363.

Li, J., Chen, C., Zhao, Y., Hu, J., Shao, D., & Wang, X. (2013). Synthesis of water-dispersible Fe_3O_4 @β-cyclodextrin by plasma-induced grafting technique for pollutant treatment. *Chemical Engineering Journal, 229*, 296–303.

Li, T., Shen, J., Huang, S., Li, N., & Ye, M. (2014). Hydrothermal carbonization synthesis of a novel montmorillonite supported carbon nanosphere adsorbent for removal of Cr (VI) from waste water. *Applied Clay Science, 93–94*(3), 48–55.

Li, X., Zhao, B., Zhu, K., & Hao, X. (2011). Removal of nitrophenols by adsorption using β-cyclodextrin modified zeolites. *Chinese Journal of Chemical Engineering, 19*(6), 938–943.

Liu, Y., Li, M., & He, C. (2016). Removal of Cr(VI) and Hg(II) ions from wastewater by novel β-CD/MGO-SO_3H composite. *Colloids & Surfaces A Physicochemical & Engineering Aspects, 512*, 129–136.

Malik, P. K. (2004). Dye removal from wastewater using activated carbon developed from sawdust: Adsorption equilibrium and kinetics. *Journal of Hazardous Materials, 113*(1–3), 81–88.

Mishra, S. R., Chandra, R., Jipsi, K. A., & Savariya, D. B. (2017). Kinetics and isotherm studies for the adsorption of metal ions onto two soil types. *Environmental Technology & Innovation, 7*, 87–101.

Qiao, J., Zhang, H. Y., & Yu, L. (2010). Synthesis of β-cyclodextrin-modified carbon nanocrystals and their fluorescent behavior. *Science Bulletin, 55*(25), 2835–2839.

Rosa, S., Laranjeira, M. C., Riela, H. G., & Fávere, V. T. (2008). Cross-linked quaternary chitosan as an adsorbent for the removal of the reactive dye from aqueous solutions. *Journal of Hazardous Materials, 155*(1–2), 253–260.

Shen, H. M., Zhu, G. Y., Yu, W. B., Wu, H. K., Ji, H. B., Shi, H. X., She, Y. B., & Zheng, Y. F. (2015). Fast adsorption of p-nitrophenol from aqueous solution using β-cyclodextrin grafted silica gel. *Applied Surface Science, 356*, 1155–1167.

Sowmya, A., & Meenakshi, S. (2013). An efficient and regenerable quaternary amine modified chitosan beads for the removal of nitrate and phosphate anions. *Journal of Environmental Chemical Engineering, 1*(4), 906–915.

Vašák, M., & Meloni, G. (2011). Chemistry and biology of mammalian metallothioneins. *JBIC Journal of Biological Inorganic Chemistry, 16*(7), 1067–1078.

Wang, G., Hua, Y., Su, X., Komarneni, S., Ma, S., & Wang, Y. (2016). Cr(VI) adsorption by montmorillonite nanocomposites. *Applied Clay Science, 124–125*, 111–118.

Xie, W., Xie, R., Pan, W., Hunter, D., Koene, B., Tan, L., & Vaia, R. (2014). Thermal stability of quaternary phosphonium modified montmorillonites. *Chemistry of Materials, 14*(11), 4837–4845.

Xing, M., & Wang, J. (2016). Nanoscaled zero valent iron/graphene composite as an efficient adsorbent for Co(II) removal from aqueous solution. *Journal of Colloid & Interface Science, 474*, 119–128.

Yan, J., Zhu, Y., Qiu, F., Zhao, H., Yang, D., Wang, J., & Wen, W. (2016). Kinetic, isotherm and thermodynamic studies for removal of methyl orange using a novel β-cyclodextrin functionalized graphene oxide-isophorone diisocyanate composites. *Chemical Engineering Research & Design, 106*, 168–177.

Yao, W., Rao, P., Lo, I. M., Zhang, W., & Zheng, W. (2014). Preparation of cross-linked magnetic chitosan with quaternary ammonium and its application for Cr(VI) and P(V) removal. *Journal of Environmental Sciences, 26*(12), 2379–2386.

Yuan, C., Liu, B., & Liu, H. (2015). Characterization of hydroxypropyl-β-cyclodextrins with different substitution patterns via FTIR, GC-MS, and TG-DTA. *Carbohydrate Polymers, 118*, 36–40.

Zhang, W., Chen, M., Gong, X., & Diao, G. (2013). Universal water-soluble cyclodextrin polymer–carbon nanomaterials with supramolecular recognition. *Carbon, 61*(5), 154–163.

Zhao, D., Zhao, L., Zhu, C., Tian, Z., & Shen, X. (2009). Synthesis and properties of water-insoluble β-cyclodextrin polymer crosslinked by citric acid with PEG-400 as modifier. *Carbohydrate Polymers, 78*(1), 125–130.

Zhao, F., Repo, E., Meng, Y., Wang, X., Yin, D., & Sillanpää, M. (2015b). An EDTA-β-cyclodextrin material for the adsorption of rare earth elements and its application in preconcentration of rare earth elements in seawater. *Journal of Colloid & Interface Science, 465*, 215–224.

Zhao, F., Repo, E., Sillanpää, M., Meng, Y., Yin, D., & Tang, W. Z. (2015c). Green synthesis of magnetic EDTA-and/or DTPA-cross-linked chitosan adsorbents for highly efficient removal of metals. *Industrial & Engineering Chemistry Research, 54*(4), 1271–1281.

Zhao, F., Repo, E., Yin, D., Meng, Y., Jafari, S., & Sillanpää, M. (2015a). EDTA-cross-linked β-cyclodextrin: An environmentally friendly bifunctional adsorbent for simultaneous adsorption of metals and cationic dyes. *Environmental Science & Technology, 49*(17), 10570–10580.

Zhao, F., Repo, E., Yin, D., & Sillanpää, M. E. (2013). Adsorption of Cd(II) and Pb(II) by a novel EGTA-modified chitosan

material: Kinetics and isotherms. *Journal of Colloid & Interface Science, 409*(11), 174–182.

Zhao, F., Tang, W. Z., Zhao, D., Meng, Y., Yin, D., & Sillanpää, M. (2014). Adsorption kinetics, isotherms and mechanisms of Cd(II), Pb(II), Co(II) and Ni(II) by a modified magnetic polyacrylamide microcomposite adsorbent. *Journal of Water Process Engineering, 4*(4), 47–57.

Zheng, W. (2001). Toxicology of choroid plexus: Special reference to metal-induced neurotoxicities. *Microscopy Research & Technique, 52*(1), 89–103.